

Morphological and dynamical properties of semiflexible filaments driven by molecular motors

Nisha Gupta,^{1,*} Abhishek Chaudhuri,^{1,†} and Debasish Chaudhuri^{2,‡}

¹*Indian Institute of Science Education and Research Mohali,
Knowledge City, Sector 81, SAS Nagar - 140306, Punjab, India.*

²*Institute of Physics, Sachivalaya Marg, Bhubaneswar 751005, India.
Homi Bhabha National Institute, Anushaktigar, Mumbai 400094, India.*

(Dated: May 11, 2022)

We consider a semiflexible filament in a gliding assay setup driven by active motor proteins. The motor proteins undergo attachment- detachment kinematics with diffusive attachment, and a detachment rate that depends on the load experienced. Attached motor proteins move along the filament to one of its ends with a velocity that varies non-linearly with the motor protein extension, the resultant force on the filament driving it out of equilibrium. The distance from equilibrium is reflected in the end-to-end distribution, modified bending stiffness, and transition to spiral morphology of the polymer. The stress dependence of activity leads to an unrestricted number of ballistic-diffusive cross-overs of the filament center of mass, limited only by observation time. This is explained using the detailed nature of the dynamics, supported by an effective active polymer description.

I. INTRODUCTION

The active cytoskeleton in a living cell provides its structural stability, mediates deformation and growth of the cell when necessary, and acts as transport lanes and highways for intracellular cargo [1, 2]. Cytoskeleton is made of semiflexible filaments, e.g., F-actins and microtubules, that are driven by associated motor proteins, for example myosin and kinesin family motor proteins respectively [3–9]. Given the complexity of the cytoskeleton in a living cell, *in vitro* experiments were devised in which purified and stabilized cytoskeletal filaments and corresponding motor proteins were studied separately [10–16]. In a gliding assay setup, heads of molecular motors are attached to a suitably prepared cover slit irreversibly, such that the tails can actively drive the associated filaments, hydrolyzing the chemical fuel ATP. This led to observation of collective motion, e.g., formation of spiral and aster patterns in microtubules driven by kinesin [12] or dynein molecules [14], or swirling patterns in high density F-actins floating on a myosin motility assay [13]. Single molecule experiments on motor proteins revealed details of their dynamics, e.g., force-velocity relation, dependence of turnover on load experienced, and dependence of activity on ATP concentration [5, 17–23]. Motion of rigid cargo under collective drive of molecular motors has been studied both experimentally and theoretically [24–32].

Related but not restricted to the above scenario, a broad field of active soft matter has seen rapid progress in recent years, due to its importance in biology and possible technological applications [33–35]. In theoretical

studies of active systems, key concepts such as broken detailed balance and entropy production has recently been used to characterize the distance of these systems from their equilibrium counterparts [36–39]. The description of such systems take two distinct approaches, meso-scale modeling in which activity and interactions are incorporated by simple rules [40–42], and hydrodynamic approach in the macroscopic limit using generic symmetry principles [33, 43, 44]. While the hydrodynamic approach captures many of the large scale properties of collective motion, understanding of specific dynamical behavior often requires a micro to mesoscopic approach, e.g., the behavior of bird flocks in the presence of a leader [45, 46], desorption of a filament from motor protein bed [47]. As we show in this paper, in the context of cytoskeletal filament- motor protein complex, description of some crucial dynamical properties requires a more microscopic approach.

Early theoretical approaches to explain experimental observations of spiral rotation or flagella like beating of a single F-actin filament in myosin gliding assay, modeled activity as a constant tangential force along the filament contour [11, 15]. Observations of emergent vortex structures in F-actin- myosin assay in Ref. [13] was explained using a hydrodynamic interaction, while the same in microtubule- dynein assay [14] was explained using polymer collision based arguments. Independent numerical simulations of self-propelled filaments are shown to spontaneously get into spiral rotation in presence and absence of hydrodynamic interaction [48–50]. Numerical simulations of active polymers composed of a permanent distribution of stresslets along its contour or chemically active / self propelled beads in the presence of hydrodynamics have shown similar results [51–54]. Generic consideration of a stiff filament in an active medium leads to the possibility of both increase or decrease of effective bending rigidity, depending on the orientation of filament segments with respect to contractile or extensile

* nishagupta@iisermohali.ac.in

† abhishek@iisermohali.ac.in

‡ debc@iopb.res.in

medium [36, 55]. The collective dynamics of such active self-propelled filaments has revealed activity driven crossovers from coherently free flowing filaments to frozen spiraling ones [56, 57]. Studies of semiflexible polymers under active correlated fluctuations showed a cross-over from bending rigidity dominated to flexible polymer-like dynamics [58]. These studies also led to prediction of a short time ballistic, to long time diffusive behavior of the mean squared displacement of polymer center of mass, showing a single crossover [50, 59].

In this paper we present numerical simulation results of an extensible semiflexible filament, explicitly modeling a motor protein gliding assay. Individual motor proteins are modeled as harmonic springs undergoing attachment-detachment kinetics that do not obey detailed balance. The attachment to filament is diffusion limited, and the detachment rate increases exponentially with the extension of individual motor proteins. In the attached state the *tail* of a motor protein moves tangentially towards one end of the polymer in an active manner, with a velocity that depends non-linearly on the motor protein extension.

We characterize the non-equilibrium conformations of the polymer comparing its end-to-end distribution with that of the equilibrium filament using a stochastic entropy difference. We show that subtle changes in the local load dependence of detachment rate and active velocity of motor proteins, leads to dramatic differences in the end-to-end distribution. As expected, the difference increases with increasing activity. The effective bending stiffness reduces, and the polymer shows a first order like conformational transition to phase coexistence between open and spiral chains with increasing activity. This result is in qualitative agreement with earlier studies on active polymers [48, 50]. The polymer morphology is determined by active velocity, turnover rates and bending rigidity of the filament. The most startling result is seen in the dynamics. The center of mass of the polymer shows a *unrestricted* number of cross-overs between ballistic and diffusive motion limited only by the observation time. To our knowledge, this kind of behavior was never reported in the literature before.

In the following section we present the detailed model. All the results are discussed in Section III. The dynamical cross-overs are analyzed with the help of individual trajectories, and an effective Langevin equation. They are understood in terms of the change in conformation, showing interesting structure- dynamics coupling.

II. MODEL AND SIMULATIONS

We consider an extensible semiflexible filament described as a bead-spring chain of N beads constituting $(N-1)$ bonds of equilibrium length σ such that the chain length $L = (N-1)\sigma$, spring constant A , and finite bend-

ing rigidity κ . This is described by the Hamiltonian

$$\beta H = \sum_{i=1}^{N-1} \frac{A}{2\sigma} [\mathbf{b}(i) - \sigma \mathbf{t}(i)]^2 + \sum_{i=1}^{N-2} \frac{\kappa}{2\sigma} [\mathbf{t}(i+1) - \mathbf{t}(i)]^2, \quad (1)$$

with $\beta = 1/k_B T$, the inverse temperature. The bond vector $\mathbf{b}(i) = \mathbf{r}(i+1) - \mathbf{r}(i)$, where $\mathbf{r}(i)$ denotes the position of the i -th bead. This allows one to define the local tangent $\mathbf{t}(i) = [\mathbf{r}(i+1) - \mathbf{r}(i)]/b(i)$. In the limit of large A , instantaneous bond lengths $b(i) \approx \sigma$, and the polymer maps to a worm like chain [60]. In addition, excluded volume interactions between the non-bonded beads of the polymer is incorporated via a Weeks-Chandler-Anderson (WCA) potential $\beta V_{WCA}(r_{ij}) = 4[(\sigma/r_{ij})^{12} - (\sigma/r_{ij})^6 + 1/4]$ if $r_{ij} < 2^{1/6}\sigma$ and 0 otherwise.

The polymer is placed on a substrate of motor protein (MP) assay. We explicitly model MPs and their dynamics, unlike several recent studies that used effective active polymer models [50, 58, 59, 61]. The MPs are modeled as *active* elastic linkers. The *head* of i -th MP is attached irreversibly to the substrate at position $\mathbf{r}_0^i = (x_0^i, y_0^i)$, while the *tail* is free to bind (unbind) to (from) the polymer. The attachment process is diffusion limited. The tail of a MP attaches to a polymer segment if it lies within a capture radius r_c with an attachment rate ω_{on} . The extension $\Delta \mathbf{r}$ of the MP in the attached state generates an elastic load $\mathbf{f}_l = -k_m \Delta \mathbf{r}$. An attached MP unbinds from a polymer segment with a rate ω_{off} which depends on the stress felt by the MP as

$$\omega_{\text{off}} = \omega_0 \exp(f_l/f_d), \quad (2)$$

where ω_0 is the bare off rate, $f_l = |\mathbf{f}_l|$ and f_d is the detachment force. The ratio $\omega_{\text{on}} : \omega_{\text{off}}$ does not obey detailed balance. When attached, a MP can move on the filament towards one of its ends, depending on the MP and filament type. For example, attached Kinesin moves towards positive end of the microtubule with *active* velocity v_t^a along the local tangent of the filament given by [21, 47]

$$v_t^a(f_t) = \frac{v_0}{1 + d_0 \exp(f_t/f_s)}, \quad (3)$$

where $f_t = -\mathbf{f}_l \cdot \mathbf{t}$, $d_0 = 0.01$ and f_s is the stall force. Here v_0 denotes the velocity of MP in the absence of stress.

We perform numerical simulations of the model to investigate structural and dynamical properties of the polymer, actively driven by MPs. The molecular dynamics of polymer is performed using the velocity-Verlet algorithm in presence of a Langevin heat bath. The bath fixes the ambient temperature $k_B T$ through a Gaussian white noise obeying $\langle \eta_i(t) \rangle = 0$, and $\langle \eta_i(t) \eta_j(t') \rangle = 2\alpha k_B T \delta_{ij} \delta(t - t')$, where α denotes viscosity of the environment. The unit of energy is set by $k_B T$, length is set by σ and time by $\tau = \alpha \sigma^2 / k_B T$. This defines a diffusion coefficient, $D = k_B T / \alpha$. In these reduced units we choose, $r_c = 0.5\sigma$, $f_s = 2k_B T / \sigma$, $f_d = f_s$, $A = 100\sigma^{-1}$, $k_m = A/\sigma$ and density of motor proteins

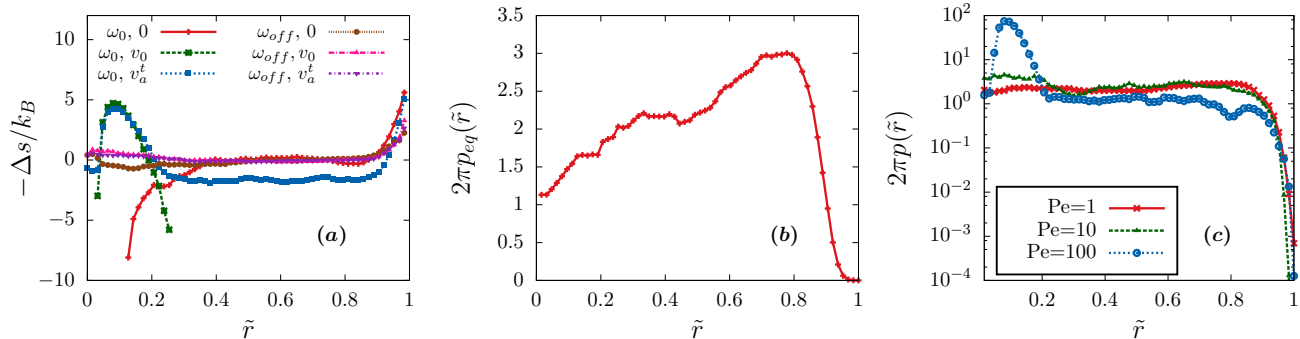


FIG. 1. (color online) Activity dependence of end-to-end distribution function $p(\tilde{r})$ at rigidity parameter $u = 3.33$ and $\Omega = 5/6$. (a) A measure of stochastic entropy difference of filament under active drive with respect to that of the equilibrium polymer. (b) End-to-end distribution of stretchable semiflexible polymer at equilibrium $p_{eq}(\tilde{r})$. (c) End-to-end distribution for three different values of Pe using stretching dependent turnover and active velocity.

in the 2d assay, $\rho = 3.8\sigma^{-2}$. In absence of MPs, the polymer shows established equilibrium properties. The attachment (detachment) of MP tails are stochastic, and performed using probabilities $\omega_{on} \delta t (\omega_{off} \delta t)$. The extension in the attached state has two contributors – the MP tail is dragged along with the filament segment to which it is attached, and it can slide from one segment to another with an active velocity v_t^a . We study the influence of the active bed of MPs on the static and dynamic properties of the polymer as we vary the (a) bare processivity $\Omega = \omega_{on}/(\omega_{off} + \omega_0)$ and (b) a dimensionless Peclet number defined as $Pe = v_0\sigma/D$.

III. RESULTS

At equilibrium, mechanical and structural properties of a semiflexible filament are determined by the persistence ratio $u = L/\lambda$, where L is the contour length of the chain, and λ is the persistence length, which for a worm-like-chain (WLC) is related to bending rigidity κ by $\lambda = 2\kappa/(d-1)$ [60]. The active drive from processive MPs attaching (detaching) to (from) the filament generates non-equilibrium stress which have profound effect on the steady state conformational properties of the polymer. To characterize the conformational properties, we obtain probability distribution of the end-to-end distance, $P(r, L)$, of the polymer. At equilibrium, this has the scaling form, $P(r, L) = \frac{1}{L^d} p(r/L, L/\lambda) = \frac{1}{L^d} p(\tilde{r}, u)$ where $\tilde{r} = r/L$ and $u = L/\lambda$. The WLC limit of our polymer model is obtained in the limit of large bond-stiffness A . In equilibrium, $p(\tilde{r}, u)$ for WLC shows a first-order-like transition from a single maximum at $\tilde{r} = 0$ for the flexible limit of large u to a maximum at $\tilde{r} = \pm 1$ for a very rigid polymer with small u [60, 62]. The transition point was determined to be near $u = 3.33$ in two and three dimensions. However, in presence of self-avoidance, the probability of end-to-end separation $p(\tilde{r}, u)$ at $\tilde{r} = 0$ gets suppressed (see Fig. 1(b)). In all our simulations, except

for in Fig. 5(b), we use $\kappa = 9.45\sigma$ that corresponds to $u = 3.33$ for $L = 63\sigma$ chains.

A. How far from equilibrium the polymer is?

Under the active drive of the gliding assay of MPs, the morphology of the polymer changes. In Fig.1 we show how this impacts the end-to-end distribution function $p(\tilde{r}, u)$. The change in the distribution function with respect to the equilibrium distribution is a measure of how far from equilibrium the polymer is, in terms of its morphology. This is well captured by the difference in *stochastic entropy* between the two states [63],

$$\Delta s = -k_B \ln \left[\frac{p(\tilde{r})}{p_{eq}(\tilde{r})} \right]. \quad (4)$$

In Fig.1(a) we show how the dimensionless quantity $-\Delta s/k_B$ changes with activity. The equilibrium distribution p_{eq} is shown in Fig.1(b).

If the activity of MPs is independent of the load force acting on them, $\omega_{off} = \omega_0$ and $v_t^a = v_0$. This corresponds to the limit of infinitely large f_d and f_s . It is expected that the deviation Δs would be large for large non-equilibrium driving, quantified in terms of large f_d , f_s and Ω .

We first consider the situation in which $\omega_{off} = \omega_0$ is kept fixed ($\omega_{on} : \omega_0 = 5 : 1$ which corresponds to $\Omega = 5/6$), and the active velocity v_t^a is varied (Fig.1(a)) for three possible situations. (i) In the absence of any directed motion of the polymer, i.e., with $v_0 = 0$, the non-equilibrium end-to-end distance distribution, with respect to the equilibrium one, shows a dip near $\tilde{r} = 0$, indicating a relative bias to the *open* conformations of the polymer. This indicates that a mere stochastic attachment/detachment kinetics of MPs, that does not obey detailed balance, leads to an enhancement of effective stiffness of the filament. (ii) When attached, MPs move but the motion is assumed to be *independent* of the load

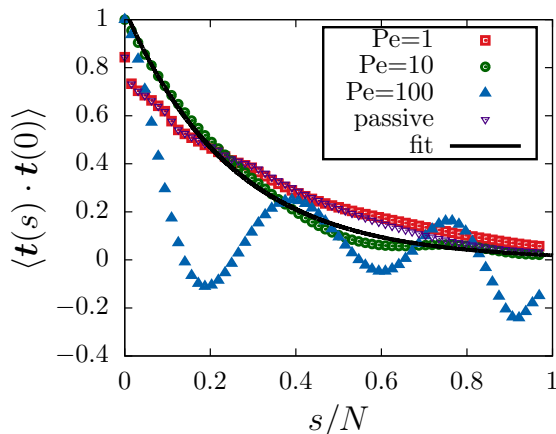


FIG. 2. (color online) Tangent-tangent correlation function for $Pe = 1, 10$ and 100 . The data set *passive* denotes equilibrium result. In presence of motor proteins the curves are for $\Omega = 5/6$. The solid line shows a single exponential fit to $Pe = 10$ data used to extract the effective persistence length $\lambda_{\text{eff}} = (15.99 \pm 0.24) \sigma$.

experienced, $v_t^a = v_0$. The effect is dramatic. The filament, gliding on the attached MPs, undergoes a transition to a rotating spiral configuration (further discussions in Sec. III C). This gives rise to a peak in the end-to-end distribution near $\tilde{r} = 0.1$, captured by the corresponding peak in $-\Delta s/k_B$. (iii) If we incorporate local stress dependence in v_t^a , the polymer is still softened but now switches between gliding and spiral states more freely. Thus in addition to the peak near $\tilde{r} = 0.1$, a non-zero probability at higher \tilde{r} appears. The statistics, dynamics and mechanical properties of the polymer under MP drive is determined by a competition between processive active velocity of MPs and bending stiffness of the polymer. The impact of this competition on end-to-end distribution is further elaborated in Appendix-A.

We next consider the situation allowing the detachment rate ω_{off} to be *dependent* on the local load force (Eq.2), and probe the regime of small Pe first. Interestingly, we find that the distribution of end-to-end distance remains largely unchanged with respect to the equilibrium behavior, with $\Delta s \approx 0$. This implies that allowing the model MPs to respond to local stress by modifying their unbinding rate is sufficient to relax the polymer morphology back towards its equilibrium conformations. In the small Pe regime, the local stress dependence/independence of the active velocity of the attached MPs, v_t^a , do not have much influence on the distribution. However, increasing Pe has a strong implication for the conformational properties as discussed in the following section.

1. Dependence on Peclet

Unlike the special cases that we considered above, real MPs do respond to MP deformations in terms of modified ω_{off} and v_a^t . Here we present conformational properties of the polymer considering these facts. Using a *bare* processivity $\Omega = 5/6$ typical for Kinesin MPs [4, 5], we investigate how polymer properties vary with increasing Pe , that might be controlled in an experiment by varying ATP concentration [21].

For low values of Pe , the local forces acting on the polymer backbone due to binding kinetics and motor movement is not sufficient to cause significant local curvature. As Pe is increased, due to tangential velocity of MPs and enhanced directional fluctuations, the polymer starts to coil up and rotates with a spiral configuration in the steady state (discussed further in Sec. III C). The impact shows up in terms of a maximum in $p(\tilde{r})$ near $\tilde{r} = 0.2$ appearing for large Peclet, $Pe = 100$ (Fig.1(c)). This feature is robust with respect to change in Ω (see Appendix-B).

B. Determination of effective stiffness

To further characterize the steady state conformational properties of the polymer, we consider the tangent-tangent correlation function, $\langle \mathbf{t}(s) \cdot \mathbf{t}(s') \rangle$ for different Pe . For an equilibrium WLC polymer, one expects a single exponential decay of the correlations, characterized by the persistence length λ as, $\langle \mathbf{t}(s) \cdot \mathbf{t}(s') \rangle = \exp(-|s - s'|/\lambda)$. Even for the driven polymer, the tangent-tangent correlation provides a measure of the structural rigidity of the filament and can also be obtained experimentally by fluorescent imaging of polymer conformations. In Fig. 2, we observe that the correlation function for small activity, $Pe = 1$, shows a characteristic exponential decay that follows the equilibrium correlation function very closely. Fig. 2 shows that the correlation length decreases with increase in Pe . This is indicative of a softening of the polymer with the emergence of strong bending fluctuations. Up to $Pe = 10$ shown in the graph, the overall nature can be described by a single exponential decay, which is fitted to extract the effective persistence length λ_{eff} , directly. For higher values of Pe , e.g., at $Pe = 100$, the correlations start showing oscillations, capturing emergence of spiral conformations that occur at higher activity. In such cases, the crossing of zero by the correlation function is interpreted as the persistence length. The variation of this effective persistence length with activity is listed in Table-I.

C. Coexistence of spiral and open chains

In order to quantify the observations of the different conformational states of the polymer, we use the turning number [64], $\psi(s) = (1/2\pi) \int_0^s ds' (\partial\theta/\partial s')$ where $\theta(s)$ is

TABLE I. Activity modulated effective persistence length of a chain of length $L = 63\sigma$ and $\kappa = 9.45\sigma$. The table shows λ_{eff} obtained from tangent-tangent correlation function. With Pe , the persistence length first increases, and then decreases.

Pe	$\lambda_{\text{eff}}/\sigma$
equilibrium	23.59 ± 0.39
1	25.21 ± 0.23
10	15.99 ± 0.24
100	8.89

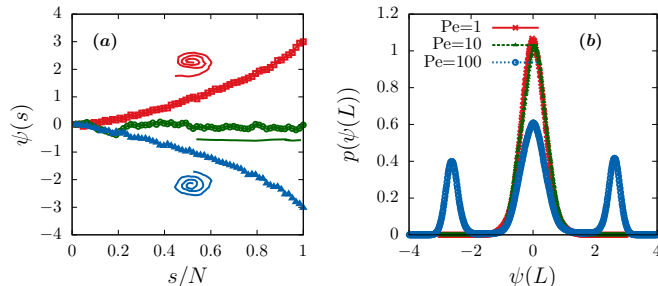


FIG. 3. (color online) (a) The turning number $\psi(s)$ plotted as a function of s for three different configurations at $Pe = 100$. It shows that $\psi(s)$ is an effective order parameter, distinguishing between the open state (green), clockwise spiral (blue) and anti-clockwise spiral (red). (b) Probability distribution for $\psi(L)$ at three different Pe and $\Omega = 5/6$.

the angle subtended by the unit tangent $\hat{t}(s)$ with x -axis. This $\psi(s)$ is a good order parameter, clearly distinguishing an open polymer from a spiral one and also separates clockwise and anticlockwise spiral states (Fig. 3(a)). The steady state probability distribution of $\psi(s = L)$ is a Gaussian with a peak at $\psi(L) = 0$ for small Pe , indicating the absence of spiral states. Increasing Pe has a dramatic effect on the distribution, with symmetric peaks emerging for non-zero $\psi(L)$ indicative of coexisting spiral states with equal probabilities of clockwise and anticlockwise winding, along with the open state characterized by $\psi(L) = 0$. Such phase coexistence is a characteristic feature of a non-equilibrium first order phase transition.

D. Anomalous dynamics of the center of mass

In Fig. 4(a) we show mean squared displacement (MSD) of the polymer center of mass as a function of time, for three different Pe values that are separated over two decades. At very short time the MSD shows an approximate *ballistic* scaling with time at all Pe . With increasing time we find several ballistic-diffusive crossovers, limited only by the total run time of our simulations. For example, the MSD for $Pe = 1$, shows ballistic-diffusive-ballistic-diffusive-ballistic crossovers. The time lag between such crossovers increases with increasing Pe , thus reducing the total number of crossovers observed over a given time window. A closer look at the *bal-*

listic regime suggests, in fact, a super-diffusive scaling $\langle (\delta r_{\text{cm}})^2 \rangle \sim \tau^{1.8}$, which we explain in the later part of this section. It is well understood that while a persistent random motion shows one ballistic-diffusive crossover, a directed random motion undergoes a single diffusive-ballistic crossover with increasing time [65]. Such behavior is a recurring feature of active systems, including active polymers [50, 59, 66]. However, unrestricted number of ballistic-diffusive cross-overs limited only by the observation time, is an effect which to our knowledge, were never reported in the literature. We first explain the reason of such a dynamic behavior resorting to a stochastic trajectory of the polymer from our simulations, followed by an approximate theoretical analysis.

Given the system spends longer time in both the ballistic and diffusive modes of dynamics at higher Pe , it is easier to find and analyze longer trajectories in each of these states at $Pe = 100$. Thus, for better clarity, in Fig. 4(b) we show time evolution of the center of mass position of the polymer at $Pe = 100$, indicating its various conformations associated with the trajectory. As the polymer takes a folded conformation, which is often a spiral in this case, the force generated in different segments by the gliding assay cancel each other, and the center of mass does not get any net directed force. As a result, the center of mass moves diffusively, getting mostly localized in a narrow region, albeit with an enhanced diffusivity due to the added active noise with respect to equilibrium (Fig. 4(b)). When the polymer retains a more open conformation, the gliding assay indeed generates directed force on the center of mass, leading to a ballistic motion over such periods shown by long directed trails in Fig. 4(b).

More quantitatively, the ballistic-diffusive crossovers can be understood by considering evolution of the end-to-end extension r_{ee} , orientation of the end-to-end vector ϕ , and the root mean squared (RMS) fluctuation of the center of mass position $\sqrt{\Delta r_{\text{cm}}^2}$ along a single trajectory (Fig. 4(c)). Clearly there are time-spans over which r_{ee} remains close to zero, i.e., in a folded (spiral at $Pe = 100$) state, e.g., between $t \approx 4.5 - 5 \times 10^5 \tau$. It should be noted that the formation of spiral happens at high Pe as was shown in Sec. III C. However, even at smaller Pe , the chain switches between open and non-spiral folded conformations. Non-spiral folds show a little higher value of r_{ee} than when spirals form.

There are other time windows over which r_{ee} fluctuates rapidly between open and spiral states (e.g., between $t \approx 0 - 4 \times 10^5 \tau$). As is shown in Fig. 4(c), ϕ changes ballistically over a timespan over which r_{ee} remains close to zero in a spiral state. In particular, between $t \approx 4.5 - 5 \times 10^5 \tau$ the angle ϕ rotates clockwise ballistically showing a linear drop in its value. During such time spans, the center of mass position of the polymer does not change appreciably, as is shown by $\sqrt{\Delta r_{\text{cm}}^2}$ in Fig. 4(c), indicating diffusion. When r_{ee} is large corresponding to open states, the gliding assay provides directed force on the center of mass. The time spans over

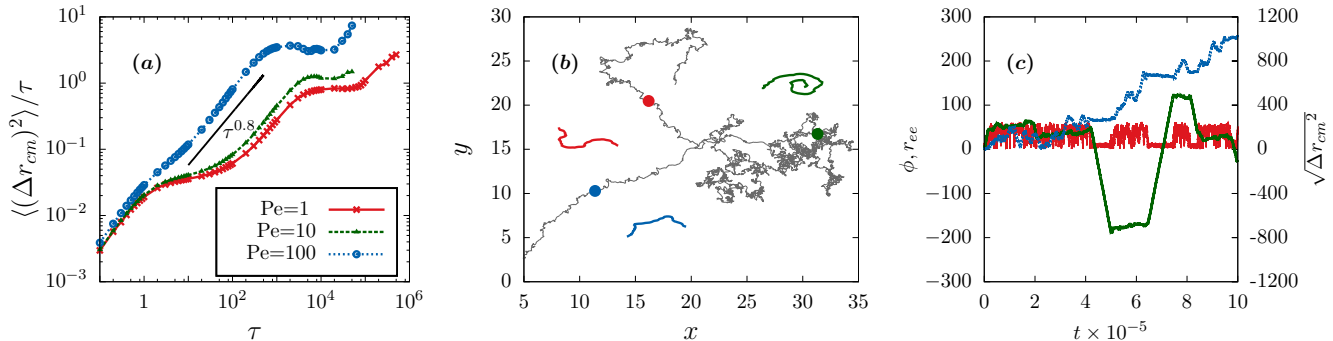


FIG. 4. (color online) Dynamics of center of mass for $\Omega = 20/21$. (a) Mean squared displacement of the center of mass at different Péclet. Numerical analysis of the dynamics at $Pe = 100$ is presented in (b) and (c). (b) The gray line shows a center of mass trajectory. Structure of polymer corresponding to the blue, red, and green points indicated on the trajectory are shown in the respective colors. (c) The end-to-end length r_{ee} (red line), end-to-end orientation ϕ (green line), and root mean squared fluctuations of the center of mass position (blue line) for a single trajectory are shown as a function of time.

which r_{ee} shows fast switching between open and folded states, $\sqrt{\Delta r_{cm}^2}$ switches rapidly between drift and diffusion. This explains an overall super-diffusive motion of the center of mass over such time spans. During such periods ϕ essentially fluctuates diffusively without any drift.

E. Effective active polymer model

The polymer under gliding assay, switching between attached and detached states, can be represented by an effective active polymer model [67], provided the attachment-detachment rates ω_{on} , $\omega_{off} (= \omega_0)$ and active velocity $v_a = v_0$ of MPs in the attached state are assumed to be independent of the MP stretching. As we have shown, in the large activity limit the effective bending rigidity gets strongly compromised. Thus ignoring bending stiffness contribution, one may write the dynamics of polymer segments $\mathbf{r}(s)$ as

$$\gamma \frac{\partial \mathbf{r}}{\partial t} = A \frac{\partial^2 \mathbf{r}}{\partial s^2} + f_p \frac{\partial \mathbf{r}}{\partial s} + \eta_a(t), \quad (5)$$

where $f_p = \gamma v_0 \Omega$ with processivity $\Omega = \omega_{on}/(\omega_{on} + \omega_{off})$. The active noise due to (de)attachment has mean $\langle \eta_a \rangle = 0$ and correlation $\langle \eta_a(s, t) \eta_a(0, 0) \rangle = D_a \exp(-t/\tau) L \delta(s)$ with noise strength $D_a = f_p^2 (\omega_{off}/\omega_{on})$ and turnover time-scale $\tau = (\omega_{on} + \omega_{off})^{-1}$. Note that in the effective dynamics, both the mean active force and strength of active noise depend on active velocity v_0 of MPs, whereas the correlation time in active noise is given by the effective turnover rate.

Analysis of the above equation in presence of f_p is not straight-forward, as the mean force acts along the local tangent that itself evolves with time. Decoupling the mean active force, and correlated random noise, as was often done in earlier publications, simplifies the analysis [58, 59]. This provides some

useful insight into the dynamical cross-overs. Using $f_p = 0$ along with a non-zero D_a allows one to expand solutions of Eq.(5) into a complete set of eigen functions $\phi_n(s) = \sqrt{2/L} \cos(n\pi s/L)$ corresponding to the eigenvalue equation $A d^2 \phi_n / ds^2 = -\epsilon_n \phi_n$, with eigen values $\epsilon_n = A(n\pi/L)^2$, and orthonormality condition $\int_0^L ds \phi_n(s) \phi_m(s) = \delta_{nm}$. The expansions $\mathbf{r}(s, t) = \sum_{n=0}^{\infty} \phi_n(s) \mathbf{r}_n(t)$, $\vec{\eta}(s, t) = \sum_{n=0}^{\infty} \phi_n(s) \vec{\eta}_n(t)$, lead to a simple relation for the center of mass position $\mathbf{r}_c(t) = \mathbf{r}_{n=0}(t) / \sqrt{2L}$. The correlation between modes $\langle \eta_m(t) \eta_n(0) \rangle = LD_a e^{-t/\tau} \delta_{m,n}$, along with the solution $\mathbf{r}_n(t) = \frac{1}{\gamma} \int_{-\infty}^t dt' e^{-(t-t')/\tau} \vec{\eta}_n(t')$, gives $(\mathbf{r}_0(t) - \mathbf{r}_0(0)) = (1/\gamma) \int_0^t dt' \vec{\eta}_0(t')$ as $\tau_0^{-1} = 0$. Finally one gets,

$$\langle [\mathbf{r}_0(t) - \mathbf{r}_0(0)]^2 \rangle = \frac{2D_a L}{\gamma^2} \left[t + \tau(e^{-t/\tau} - 1) \right].$$

As it is clear, in the short time limit $t \ll \tau$ this predicts a ballistic behavior $\langle [\mathbf{r}_c(t) - \mathbf{r}_c(0)]^2 \rangle \approx (D_a L / \gamma^2 \tau) t^2$, whereas in the long time limit $t \gg \tau$ that crosses over to normal diffusion, $\langle [\mathbf{r}_c(t) - \mathbf{r}_c(0)]^2 \rangle \approx (2D_a L / \gamma^2) t$ [59].

It is easy to show that in the presence of a thermal noise with $\langle \eta_{th}(s, t) \eta_{th}(0, 0) \rangle = 2D_{th} \delta(t) L \delta(s)$, fluctuations $\langle [\mathbf{r}_0(t) - \mathbf{r}_0(0)]^2 \rangle = 2LD_{th} t / \gamma^2$. As a result, the full expression for displacement fluctuations is

$$\langle [\mathbf{r}_c(t) - \mathbf{r}_c(0)]^2 \rangle = \frac{2D_{th} L}{\gamma^2} t + \frac{2D_a L}{\gamma^2} \left[t + \tau(e^{-t/\tau} - 1) \right] \quad (6)$$

Thus at short time, $t \ll \tau$, the overlap of ballistic and diffusive behavior $\langle [\mathbf{r}_c(t) - \mathbf{r}_c(0)]^2 \rangle = (2D_{th} L / \gamma^2) t + (D_a L / \gamma^2 \tau) t^2$ predicts an overall super-diffusive dynamics, which crosses over to diffusive scaling with an enhanced diffusion constant $2L(D_{th} + D_a) / \gamma^2$ at longer time $t \gg \tau$. This explains a single crossover from super-diffusion to diffusion with increase in time. The question is what might have led to unrestricted numbers of cross-overs as observed in our simulations.

To understand that one must resort back to the origin of the active noise (and force). Note that $D_a =$

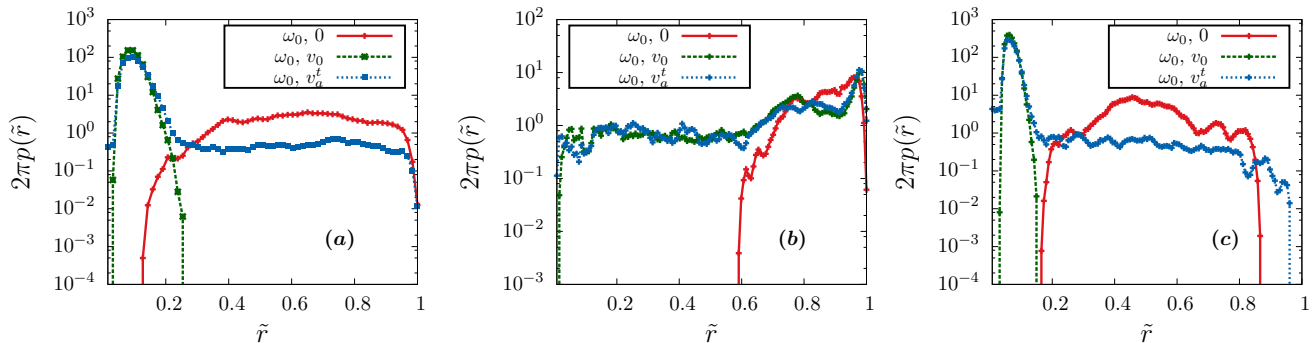


FIG. 5. (color online) End-to-end distribution at $\Omega = 5/6$. Here, we use $v_0 = 1.0 (D/\sigma)$ for all cases of non-zero active velocity, and v_a^t denotes load dependent active velocity as in Eq.3. The three graphs show results for (a) $N = 64$, $u = 3.33$, $\kappa = 9.45 \sigma$. (b) $N = 128$, $u = 3.33$, $\kappa = 19.07 \sigma$ (c) $N = 128$, $u = 6.7$, $\kappa = 9.45 \sigma$.

$\frac{\omega_{\text{on}}\omega_{\text{off}}}{(\omega_{\text{on}}+\omega_{\text{off}})^2} \gamma^2 v_a^2$, where $v_a = v_0$ is the active velocity. Although we assumed $\omega_{\text{off}} = \omega_0$ and v_a to be constants in the above analysis, in fact, for MPs they do depend on the molecular deformation. With increased f_l , ω_{off} grows exponentially, and $D_a \sim v_a^2/\omega_0$ becomes vanishingly small. Subsequent complete detachment of filament allows it to perform passive diffusion, and the load on MPs gets released. This allows MPs to reattach, starting the cycle of active ballistic to diffusive cross-overs all over again. A more quantitative theoretical analysis will require solution of the effective Langevin equation incorporating the presence of f_p and bending rigidity explicitly.

IV. DISCUSSION AND OUTLOOK

Using stochastic molecular dynamics simulations we have investigated the conformational and dynamical properties of a semiflexible polymer in the presence of motor proteins, which (un)bind (from)to the polymer and perform directed active motion. Unlike in equilibrium worm like chain, the end-to-end statistics is not controlled by the ratio of persistence length and chain length, but results from a competition between the processive active velocity and bending rigidity. The activity influences polymer morphology, mechanical properties, and dynamics in a concerted manner. With increasing activity of motor proteins, we obtained the following : (i) studies of end-to-end distribution and tangent-tangent correlation function showed an increase in the probability of small end-to-end distance associated with decrease in effective bending stiffness, (ii) with increasing activity we found onset of spiral conformations coexisting with open chains, (iii) the center of mass motion showed a unrestricted number of ballistic- diffusive crossovers with time. While some of these behaviors, e.g., formation of spiral chains at high activity was predicted within active polymer models [50], the dramatic effect of unrestricted number of ballistic- diffusive crossovers could not be described without explicit consideration of motor proteins.

This necessarily depends on stress build up and relaxation mediated by the load dependence of turnover and active velocity.

We hope our work will motivate further experimental and theoretical work on semiflexible filaments in gliding assays. Our predictions, including that on the center of mass dynamics, may be tested in microtubule-kinesin assays, or F-actin in a processive myosin-V assay.

APPENDIX A: COMPETITION BETWEEN ACTIVITY AND BENDING STIFFNESS

For a semiflexible polymer in equilibrium, the end-to-end distribution $p(\tilde{r}, u)$ is determined by the dimensionless ratio $u = L/\lambda$. On the other hand, in presence of motor proteins, the statistical and mechanical properties are expected to be determined by an interplay of activity and bending rigidity. To probe that within our model, here, we fix $\omega_{\text{off}} = \omega_0$, and vary the chain length $L = (N - 1)\sigma$ by changing N , the ratio $u = L/\lambda$, and bending rigidity κ of the polymer to study their impact on conformational properties. We use both stress dependent and independent v_a^t , and plot the end-to-end distributions for three different active velocities in Fig. 5. A comparison of Figs. 5 (a) and (b) clearly shows that for the same u and different L , unlike in equilibrium WLC, the conformational properties of the polymer are significantly different. For example, for $N = 128$ and $u = 3.33$ (Fig. 5(b)), the distribution for $v_0 = 0$ indicates a much stiffer polymer compared to $N = 64$ (Fig. 5(a)). For non-zero active velocity, the spiral states observed for $N = 64$ disappears for $N = 128$, leading to stiffer conformations devoid of spirals. If, however, we keep the value of κ fixed as we change the length of the polymer from $N = 64$ to $N = 128$ (Fig. 5(c)), the distributions we get compares much better with Fig. 5(a). This shows that, for a given processivity Ω , the conformational properties of polymers driven by MPs are determined by a competition between active velocity and bending rigidity.

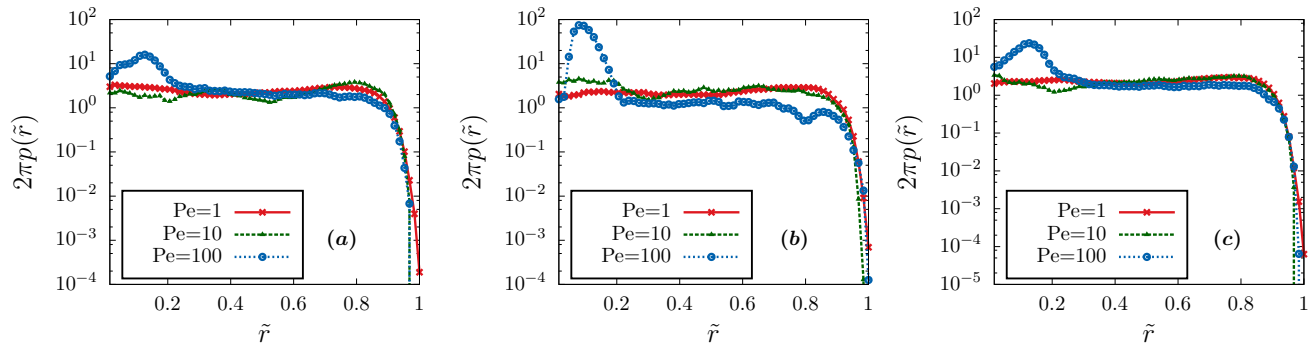


FIG. 6. (color online) End-to-end distribution at $Pe = 1, 10, 100$ for different values of bare processivity Ω , using stress dependent active velocity and detachment rate. The graphs correspond to (a) $\Omega = 2/3$, (b) $\Omega = 5/6$, and (c) $\Omega = 20/21$.

Within active polymer models having tangential drive, arguing that active force f_p may generate compression, a torque balance leads to a critical active force $f_p^c \sim \kappa/L^3$, beyond which straight filaments are unstable towards buckling [53]. In the limit of stress independent activity, a simple extension of this relation to the instability of the filament under MP driving can be obtained by replacing $f_p^c = \gamma\Omega v_0^c$ (see Sec.III E). This leads to a relation $v_0^c \sim \kappa/\gamma\Omega L^3$. Thus buckling instabilities are expected to be controlled by the dimensionless number $\mathcal{F} = \gamma\Omega v_c L^3/\kappa k_B T$. However, for polymers driven by real MPs that shows stress dependent activity, the determining factors are expected to be more subtle, and remains to be studied in future.

APPENDIX B: END-TO-END DISTRIBUTIONS FOR DIFFERENT Ω

In Fig. 6, we show the dependence of the conformational properties of the polymer as the bare processivity $\Omega = \omega_{on}/(\omega_{on} + \omega_0)$ is varied. Here we consider the scenario where both the detachment rate and the active

velocity depend on the local stress. For a fixed Ω we plot the end-to-end distribution of the polymer as Pe is changed. As in Fig. 1(c), the distributions look similar to equilibrium distribution $p(\tilde{r})$ for low Pe and a peak near $\tilde{r} \approx 0$ appears for high Pe , indicating the emergence of spiral states. Therefore we conclude that for stress dependent ω_{off} , varying Ω does not affect the conformational properties significantly. Recall that a stress independent ω_{off} with non-zero Pe results in coiled states of the polymer. Switching on local stress dependence in ω_{off} allows the polymer to relax back to its equilibrium conformations whenever stress builds up beyond a limit, even if the processivity Ω is high. As Pe is increased, it triggers an instability towards spiral states and we see the emergence of a peak near $\tilde{r} = 0$ in the steady state distributions.

ACKNOWLEDGEMENTS

A.C and D.C. acknowledge SERB, India for financial support through grant number EMR/2014/000791. DC thanks SERB, India, for financial support through grant number EMR/2016/001454, and ICTS-TIFR, Bangalore for an associateship. N.G. acknowledges UGC, India for a fellowship.

-
- [1] J. Howard, *Handbook of Complex Variables* (OUP, USA, 2005).
 - [2] B. Alberts, D. Bray, K. Hopkins, A. Johnson, J. Lewis, M. Raff, K. Roberts, and P. And Walter, *Arch. Biochem. Biophys.* (PUBLISHER, ADDRESS, 2009), Vol. 231, p. 860.
 - [3] R. D. Vale, *Cell* **112**, 467 (2003).
 - [4] D. Chowdhury, *Phys. Rep.* **529**, 1 (2013).
 - [5] W. O. Hancock and J. Howard, *Proc. Natl. Acad. Sci.* **96**, 13147 (1999).
 - [6] D. A. Fletcher and R. D. Mullins, *Nature* **463**, 485 (2010).
 - [7] F. Huber, J. Schnauß, S. Rönicke, P. Rauch, K. Müller, C. Fütterer, and J. Käs, *Adv. Phys.* **62**, 1 (2013).
 - [8] F. C. MacKintosh, J. Käs, and P. a. Janmey, *Phys. Rev. Lett.* **75**, 4425 (1995).
 - [9] H. Yamaoka, S. Matsushita, Y. Shimada, and T. Adachi, *Biomech. Model. Mechanobiol.* **11**, 291 (2012).
 - [10] S. J. Kron and J. a. Spudich, *Proc. Natl. Acad. Sci. U. S. A.* **83**, 6272 (1986).
 - [11] K. Sekimoto, N. Mori, K. Tawada, and Y. Y. Toyoshima, *Phys. Rev. Lett.* **75**, 172 (1995).
 - [12] T. Surrey, F. Nédélec, S. Leibler, and E. Karsenti, *Science* **292**, 1167 (2001).
 - [13] V. Schaller, C. Weber, C. Semmrich, E. Frey, and A. R. Bausch, *Nature* **467**, 73 (2010).
 - [14] Y. Sumino, K. H. Nagai, Y. Shitaka, D. Tanaka, K. Yoshikawa, H. Chaté, and K. Oiwa, *Nature* **483**, 448

- (2012).
- [15] L. Bourdieu, T. Duke, M. B. Elowitz, D. A. Winkelmann, S. Leibler, and A. Libchaber, *Phys. Rev. Lett.* **75**, 176 (1995).
- [16] J. Kierfeld, K. Frentzel, P. Kraikivski, and R. Lipowsky, *Eur. Phys. J. Spec. Top.* **157**, 123 (2008).
- [17] K. Oiwa, S. Chaen, E. Kamitsubo, T. Shimmen, and H. Sugi, *Proc. Natl. Acad. Sci. U. S. A.* **87**, 7893 (1990).
- [18] D. L. Coy, M. Wagenbach, and J. Howard, *J. Biol. Chem.* **274**, 3667 (1999).
- [19] A. D. Mehta, R. S. Rock, M. Rief, J. a. Spudich, M. S. Mooseker, and R. E. Cheney, *Nature* **400**, 590 (1999).
- [20] M. Rief, R. S. Rock, A. D. Mehta, M. S. Mooseker, R. E. Cheney, and J. A. Spudich, *Proc. Natl. Acad. Sci.* **97**, 9482 (2000).
- [21] M. J. Schnitzer, K. Visscher, and S. M. Block, *Nat. Cell Biol.* **2**, 718 (2000).
- [22] R. S. Rock, S. E. Rice, a. L. Wells, T. J. Purcell, J. a. Spudich, and H. L. Sweeney, *Proc. Natl. Acad. Sci. U. S. A.* **98**, 13655 (2001).
- [23] A. Yildiz, J. N. Forkey, S. a. McKinney, T. Ha, Y. E. Goldman, and P. R. Selvin, *Science* **300**, 2061 (2003).
- [24] S. P. Gross, M. Carolina Tuma, S. W. Deacon, A. S. Serpinskaya, A. R. Reilein, and V. I. Gelfand, *J. Cell Biol.* **156**, 855 (2002).
- [25] C. Kural, H. Kim, S. Syed, G. Goshima, V. I. Gelfand, and P. R. Selvin, *Science* **308**, 1469 (2005).
- [26] F. Jülicher and J. Prost, *Phys. Rev. Lett.* **75**, 2618 (1995).
- [27] A. Vilfan, E. Frey, and F. Schwabl, *Eur. Phys. J. B* **3**, 535 (1998).
- [28] M. Badoual, F. Jülicher, and J. Prost, *Proc. Natl. Acad. Sci. U. S. A.* **99**, 6696 (2002).
- [29] S. Grill, K. Kruse, and F. Jülicher, *Phys. Rev. Lett.* **94**, 108104 (2005).
- [30] S. Klumpp and R. Lipowsky, *Proc. Natl. Acad. Sci.* **102**, 17284 (2005).
- [31] C. Leduc, N. Pavin, F. Jülicher, and S. Diez, *Phys. Rev. Lett.* **105**, 128103 (2010).
- [32] A. Nair, S. Chandel, M. K. Mitra, S. Muhuri, and A. Chaudhuri, *Phys. Rev. E* **94**, 032403 (2016).
- [33] M. C. Marchetti, J. F. Joanny, S. Ramaswamy, T. B. Liverpool, J. Prost, M. Rao, and R. A. Simha, *Rev. Mod. Phys.* **85**, 1143 (2013).
- [34] C. Bechinger, R. Di Leonardo, H. Löwen, C. Reichhardt, G. Volpe, and G. Volpe, *Rev. Mod. Phys.* **88**, 045006 (2016).
- [35] J. Elgeti, R. G. Winkler, and G. Gompper, *Reports on Progress in Physics* **78**, 056601 (2015).
- [36] J. Gladrow, N. Fakhri, F. C. Mackintosh, C. F. Schmidt, and C. P. Broedersz, *Phys. Rev. Lett.* **116**, (2016).
- [37] É. Fodor, C. Nardini, M. E. Cates, J. Tailleur, P. Visco, and F. van Wijland, *Phys. Rev. Lett.* **117**, 038103 (2016).
- [38] C. Ganguly and D. Chaudhuri, *Phys. Rev. E* **88**, 032102 (2013).
- [39] D. Chaudhuri, *Phys. Rev. E* **90**, 022131 (2014).
- [40] T. Vicsek, A. Czirók, E. Ben-Jacob, I. Cohen, and O. Shochet, *Phys. Rev. Lett.* **75**, 1226 (1995).
- [41] F. Ginelli, F. Peruani, M. Bär, and H. Chaté, *Phys. Rev. Lett.* **104**, 184502 (2010).
- [42] T. Vicsek and A. Zafeiris, *Phys. Rep.* **517**, 71 (2012).
- [43] F. Jülicher, S. W. Grill, and G. Salbreux, *Reports Prog. Phys.* **81**, 076601 (2018).
- [44] S. Ramaswamy, *Journal of Statistical Mechanics: Theory and Experiment* **2017**, 054002 (2017).
- [45] A. Flack, M. Nagy, W. Fiedler, I. D. Couzin, and M. Wikelski, *Science* **360**, 911 (2018).
- [46] A. M. Berdahl, A. B. Kao, A. Flack, P. A. H. Westley, E. A. Codling, I. D. Couzin, A. I. Dell, and D. Biro, *Philos. Trans. R. Soc. B Biol. Sci.* **373**, 20170009 (2018).
- [47] A. Chaudhuri and D. Chaudhuri, *Soft Matter* **12**, 2157 (2016).
- [48] H. Jiang and Z. Hou, *Soft Matter* **10**, 9248 (2014).
- [49] H. Jiang and Z. Hou, *Soft Matter* **10**, 1012 (2014).
- [50] R. E. Isele-Holder, J. Elgeti, and G. Gompper, *Soft Matter* **11**, 7181 (2015).
- [51] G. Jayaraman, S. Ramachandran, S. Ghose, A. Laskar, M. S. Bhamla, P. B. S. Kumar, and R. Adhikari, *Phys. Rev. Lett.* **109**, 158302 (2012).
- [52] A. Laskar, R. Singh, S. Ghose, G. Jayaraman, P. B. S. Kumar, and R. Adhikari, *Sci. Rep.* **3**, 1964 (2013).
- [53] R. Chelakkot, A. Gopinath, L. Mahadevan, and M. F. Hagan, *Journal of The Royal Society Interface* **11**, (2014).
- [54] D. Sarkar and S. Thakur, *The Journal of Chemical Physics* **146**, 154901 (2017).
- [55] N. Kikuchi, A. Ehrlicher, D. Koch, J. a. Käs, S. Ramaswamy, and M. Rao, *Proc. Natl. Acad. Sci. U. S. A.* **106**, 19776 (2009).
- [56] K. R. Prathyusha, S. Henkes, and R. Sknepnek, *Phys. Rev. E* **97**, 022606 (2018).
- [57] . Duman, R. E. Isele-Holder, J. Elgeti, and G. Gompper, *Soft Matter* **14**, 4483 (2018).
- [58] T. Eisenstecken, G. Gompper, and R. Winkler, *Polymers (Basel)*. **8**, 304 (2016).
- [59] A. Ghosh and N. S. Gov, *Biophys. J.* **107**, 1065 (2014).
- [60] A. Dhar and D. Chaudhuri, *Phys. Rev. Lett.* **89**, 65502 (2002).
- [61] Y. Yang, V. Marceau, and G. Gompper, *Phys. Rev. E* **82**, 1 (2010).
- [62] D. Chaudhuri, *Phys. Rev. E* **75**, 21803 (2007).
- [63] U. Seifert, *Rep. Prog. Phys.* **75**, 126001 (2012).
- [64] S. G. Krantz, *Handbook of Complex Variables* (Birkhäuser, Boston, MA, 1999).
- [65] F. Peruani and L. G. Morelli, *Phys. Rev. Lett.* **99**, 010602 (2007).
- [66] D. Selmeczi, S. Mosler, P. H. Hagedorn, N. B. Larsen, and H. Flyvbjerg, *Biophys. J.* **89**, 912 (2005).
- [67] C. Gardiner, *Stochastic Methods: A Handbook for the Natural and Social Sciences, Springer Series in Synergetics* (Springer Berlin Heidelberg, ADDRESS, 2009).